NANO LETTERS

pubs.acs.org/NanoLett Letter

Atomically Precise Nanoclusters as SERS Probes

Sujan Manna, Anant O. Bhasin, Vivek Yadav, Soham Chowdhury, Subrata Duary, Samapti Mondal, Sajal Kumar Giri, Tomas Base,* George C. Schatz,* and Thalappil Pradeep*

Cite This: https://doi.org/10.1021/acs.nanolett.5c05462 Read Online

ACCESS | Metrics & More | Article Recommendations | Supporting Information

ABSTRACT: Atomically precise nanoclusters (NCs) exhibit molecule-like fingerprints, yet their Raman response is usually buried under intense luminescence. Herein, we report the use of surface-enhanced Raman spectroscopy (SERS) to probe the molecular nature of the stable eight-electron silver NC, $[Ag_{17}(o_1\text{-carboranethiolate})_{12}]^{3-}$ (abbreviated as Ag_{17}), by integrating it with plasmonic gold nanotriangles (Au NTs), forming an Ag_{17}@Au NT nanohybrid. This is the first demonstration of an atomically precise NC functioning as a stable next-generation Raman probe under harsh laser conditions. Synergistic electromagnetic (EM) and chemical enhancement (CE) mechanisms yield an overall enhancement factor of up to $\sim 6 \times 10^5$, with $\sim 2 \times 10^2$ attributed to CE, consistent with time-dependent density functional theory (TDDFT) calculations. TDDFT reproduces the observed spectra and reveals low-lying hybrid charge-transfer excited states, underpinning the CE pathway. Plasmonic confinement and charge transfer cooperatively amplify the Raman scattering of the Ag−Ag bonds and carborane framework at the nanoscale junctions of the Ag_{17}@Au NT nanohybrid.

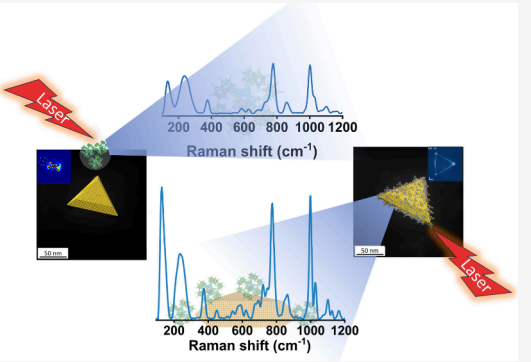

KEYWORDS: *nanoclusters, surface-enhanced Raman spectroscopy, chemical enhancement, nanohybrid, anisotropic nanoparticles*

Surface-enhanced Raman spectroscopy (SERS) is a surface-sensitive technique in which metal nanostructures concentrate the electromagnetic (EM) field at their surface, thereby contributing to signal enhancement.[1−3] The chemical enhancement (CE) mechanism of SERS depends on the electronic pull and push between the metals and the probes.[4,5] The charge transfer (CT) depends on the relative alignment between the Fermi level of the metal and the frontier orbital of the adsorbed molecule.[6,7] Similar to the CT enhancement strategies employed in semiconductors and 2D materials,[8−10] NCs have been used to modulate CT in nanoparticle systems to enhance SERS signals.[11]

Noble metal NCs,[12−15] bridging molecules and plasmonic nanocrystals in physical dimensions, possess atomic precision and have unique optical properties.[16−19] Several Ag NCs with well-defined molecular formulas have been synthesized.[20−27] Although Ag NCs are typically less stable and more sensitive to environmental factors,[28] stability can be enhanced significantly through careful ligand design, as in $[Ag_{17}(o_1\text{-carboranethiolate})_{12}]^{3-}$ (abbreviated as Ag_{17}), which is stable up to 125 °C in the solid state.[29] The emergence of carboranethiol-protected NCs offers new possibilities due to their enhanced stability.[23,30] The free *o*-carborane cage attains a high polarity, with a dipole moment of about 4.45 D.[31] Carboranes (CBs), characterized by robust σ-aromatic bonding and electron-deficient skeletal frameworks,[32] act as strong substituents that promote interfacial CT.[30,33,34]

Gold nanotriangles (Au NTs) have strong localized surface plasmon resonance (LSPR) and are favored in SERS due to their sharp vertices and edges.[35,36] NTs outperform spheres and spherical aggregates due to their anisotropy.[37−39]

Extending this anisotropy effect, nonoverlapping LSPR with Ag_{17} absorption and CT, we coupled Ag_{17} NCs with Au NTs to show that NCs can act as molecular probes for SERS with a quantifiable CE. Traditional SERS reporter molecules, such as 4-aminothiophenol (4-ATP) and dyes like rhodamine derivatives, often suffer from photodegradation, photooxidation, and dynamic binding.[40,41] Moreover, small probe molecules can adsorb in different orientations on metal surfaces,[42,43] leading to unpredictable SERS selection rules and intensity variations. In contrast, the Ag_{17} cluster is an ∼1.7 nm multiligand entity that anchors to Au NTs, forming atomically precise interfaces via multiple weak interactions, e.g., electrostatic attraction of its anionic shell to the CTAC-stabilized Au surface. This multivalent adsorption, along with the rigid carborane-cage ligand structure, results in a more fixed orientation and a more stable spectral output.

Received: October 31, 2025
Revised: March 6, 2026
Accepted: March 6, 2026

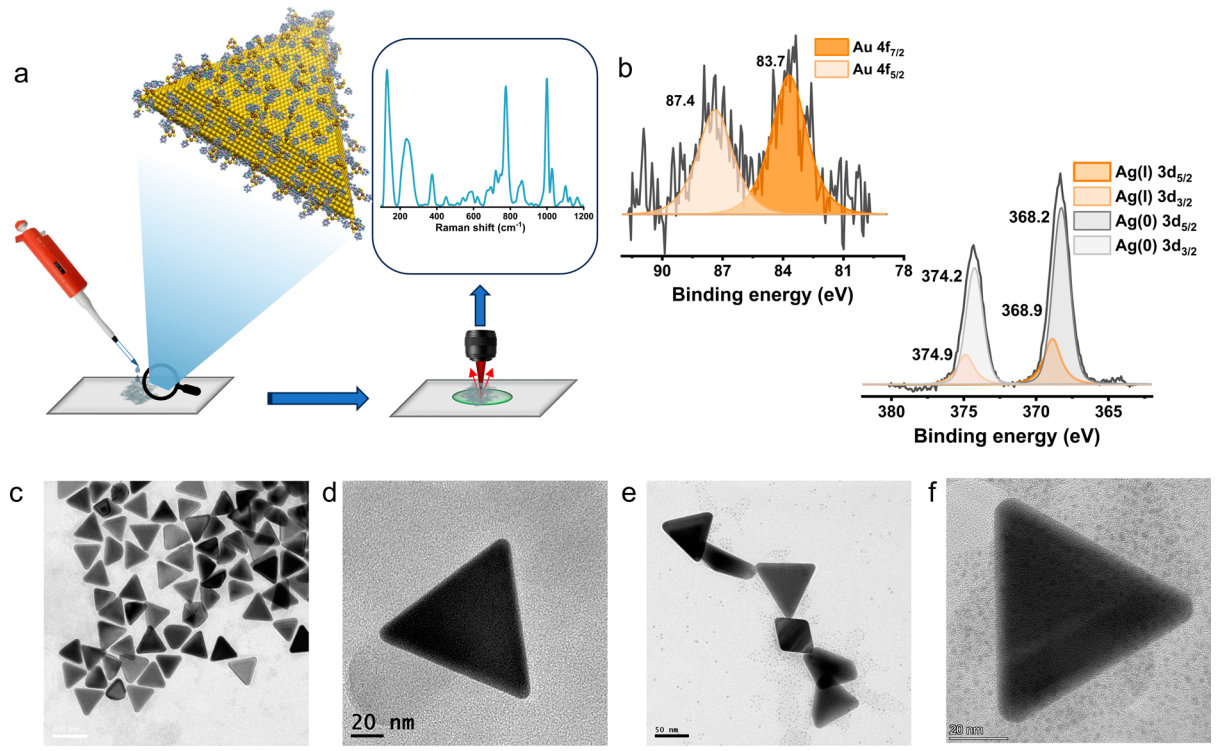

Figure 1. Ag_{17}@Au NT nanohybrid platform: concept, interfacial speciation, and morphology. (a) Schematic illustration of the workflow for Ag_{17} on Au NTs with a representative spectrum. (b) XPS of the nanohybrid in the Au 4f region, consistent with metallic Au (top left); Ag 3d region deconvoluted into Ag(I) and Ag(0), confirming thiolate-bound Ag (bottom right). (c-f) TEM images: (c) Overview of uniform Au NTs. (d) High-magnification TEM image of the Au NT with flat facets and sharp vertices. (e) TEM image of the Ag_{17}@Au NT, with different orientations exposed to the electron beam. (f) High-magnification TEM image of the Ag_{17}@Au NT showing Ag NCs on hot spots and flat faces.

Consequently, the NC−NP nanohybrids yield synergistic charge-transfer and field effects. These effects result in an enhancement factor (EF) of ~6 × 10^5, calculated using established SERS quantification methods,[44] with a relative standard deviation (RSD) of 9.1% and a detection limit of 1.64 nM. Time-dependent density functional theory (TDDFT) and finite-difference time-domain (FDTD) simulations reveal that low-lying hybrid charge-transfer states drive the chemical pathway, while plasmonic coupling at NT tips provides localized field amplification. These combined effects establish a reproducible, luminescence-free SERS platform that converts NCs into next-generation molecular reporters for precision sensing. However, reproducibility at scale requires stabilization of the nanocluster−nanoparticle (NC−NP) interface to minimize spectral variance across probe populations. Recent developments in molecular tethering, surface functionalization,[45] self-assembled monolayer (SAM) engineering, alloyed anisotropic nanoparticles,[46] nanoshell encapsulation,[47,48] and ligand-exchange chemistry[29] enable reproducible interparticle architectures. Such precision nanostructures have the potential to function as new diagnostic tools in areas such as quantum sensors, molecular electronics, and interdigitated nanoelectrode arrays.

Planar Au NTs (with an edge length of ~72.5 nm), synthesized by the Scarabelli protocol,[49] showed a uniform morphology (Figures S1 and S2), while Ag_{17}, prepared by Yadav's method,[29] was characterized by UV−vis, ESI-MS, and XPS (Figures S3, S4, and S5a). UV−vis measurements showed that Ag_{17} exhibited bands at 400, 312, 268, and 240 nm, consistent with the reported values.[29] PL measurements confirmed negligible visible emission (Figure S3c) and good Raman scattering (Figure S6), in contrast to those of several NCs. The synthetic protocols are described in detail in the Experimental procedures of the Supporting Information.

For SERS measurments, Ag_{17} crystals, prepared by slow evaporation of DCM, were dissolved in ethanol to ensure that Au NTs were unaffected upon contact with the cluster solution. Figure 1a schematically shows the drop casting of Ag_{17} on a Au NT-covered glass substrate; the latter was immobilized using 3-mercaptopropyltrimethoxysilane (MPTMS) functionalization. MPTMS provided thiol functionalities for anchoring Au NTs. A minimal dose of MPTMS (0.5% (v/v)) was employed, sufficient to promote stable adhesion of the Au NTs, while ensuring that no detectable Raman signal from the silane layer contributed to the measurements. The spectrum, along with the schematic (Figure 1a), represents Ag_{17} as a Raman probe. The oxidation states of Ag and S are vital, and any change in these can dictate the loss of structural integrity and hence the change or breakdown of the NCs during nanohybrid formation. The peak positions, indicating the immediate environment and the intensity ratio of Ag(0) to Ag(I) were unaltered after the formation of the nanohybrid. In the bottom right corner of Figure 1b, XPS of Ag_{17}@Au NT showed no observable Au−Ag exchange. The Ag(0) peaks at 374.2 and 368.2 eV and Ag(I) peaks at 374.9 and 368.9 eV, corresponding to $3d_{3/2}$ and $3d_{5/2}$, respectively, with an 80:20 Ag(0):Ag(I) ratio match precisely with the parent Ag_{17} NC (in Figure S4). A similar trend of no exchange of atoms was observed in $4f_{5/2}$ and $4f_{7/2}$ of Au NT with the presence of 87.4 and 83.7 eV peaks, respectively, as shown at the top left of Figure 1b. This rules out cluster fragmentation to form individual ligands or Ag atoms, which

https://doi.org/10.1021/acs.nanolett.5c05462
Nano Lett. XXXX, XXX, XXX−XXX

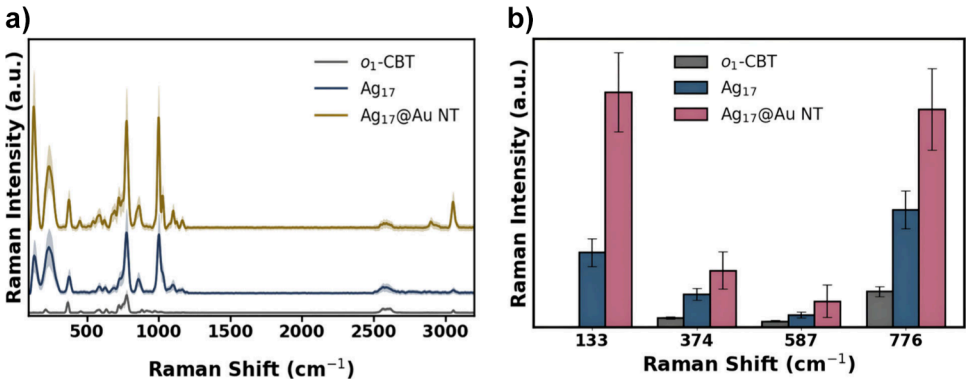

Figure 2. SERS signatures and mode quantification for Ag_{17}@Au NTs. (a) Comparative Raman overlays of the Ag_{17}@Au NT, Ag_{17}, and o_1-CBT under identical conditions. (b) Comparison of the intensities of various modes (at 133, 374, 587, and 776 cm^{-1}) for the three entities. Together, these panels demonstrate a molecular fingerprint of Ag_{17}@Au NTs and provide a basis for assignment and subsequent EM analyses. One hundred spectra were collected per sample to calculate the mean and standard deviation.

detach to bind Au NT. This is also confirmed by the absence of a Au−S signature in XPS (Figure 1 and Figure S5b).[50] This validates the protective role of the CBT ligands. High-resolution TEM (by drop casting NCs on a NT-covered TEM grid) provides direct visualization of the adsorption geometry, lattice continuity, and local contrast variations, validating that hybrid formation occurs without morphological distortion. Panels c and d of Figure 1 present the TEM images of Au NTs before Ag_{17} addition. Panels d and f of Figure 1 show the immediate environment of a single Au NT before and after the Ag_{17} addition. Tiny dark spots or contrast differences at the Au NT edges and flat surfaces mark the presence of Ag_{17} clusters (Figure 1e,f). The NCs, ranging from 1 to 2.2 nm in diameter,[12] can perfectly fit into the hot spots created by NTs. Moreover, Au NTs offer a large, atomically flat (111) facet area, where clusters can adsorb without severe structural distortion. It can create more chances for van der Waals-type interactions with the shell, driving physisorption. This interfacial confinement creates a synergistic environment for a few of the o_1-carboranethiolate (o_1-CBT) ligands, sandwiched between the Au NT and Ag_{17} metal core.

The prepared nanohybrid is expected to enhance the Raman scattering of o_1-CBT owing to its specific geometry and interface. Accordingly, we started with a solution-based SERS detection protocol using a Au NT colloidal system. The SERS spectra were recorded in a confocal microscope-based Raman spectrometer with a 633 nm laser, which is resonant with the LSPR of the Au NT at 638 nm, as shown in Figure S1a, and is off-resonant with the electronic transitions of Ag_{17}. In Figure 2a, the comparison of Raman spectra of the free ligand, the NC (10 mM), and the NC−NP nanohybrid with a concentration of 1 μM unveils a sequential 2-fold increment of spectral intensity. Raman spectra were recorded at 25 distinct positions from drop casting of Ag_{17} (Figure S7) and the Ag_{17}@Au NT nanohybrid (Figure S8) on glass substrates. The incident laser power of 0.2 mW on the sample was kept constant throughout the measurements to avoid power-induced spectral variations. Moreover, the photostability of the Ag_{17}@Au NT was examined under continuous laser exposure at 0.01 mW/cm^2 for 20 min, as shown in Figure S9. The major peaks of NC remain stable, and the relative intensities of the peaks are almost invariant, although their intensities decrease gradually over time. In addition, a calibration strategy has been performed to account for variations in the local optical fields at plasmonic hot spots, as shown in Figures S10−S13. Following the internal standard protocol reported by Lorén et al.,[51] 4-cyano-*N*-(2-mercaptoethyl) benzamide (CMEB) was employed as a thiolated self-assembled monolayer internal standard, exploiting its CN stretching band in the spectrally silent region at 2300 cm^{-1} to enable robust normalization against fluctuating SERS enhancement. The Ag_{17} NC was treated analogously to the Au NT, as described in the reference, thereby ensuring firm chemisorption of the CMEB layer via metal−sulfur bonding and minimizing competitive adsorption.

Figure 2b shows variations in the major peaks, reflecting the SERS behavior. The Raman intensities of the characteristic peaks at 133, 374, 587, and 776 cm^{-1} were compared across the free ligand, Ag_{17} NC, and Ag_{17}@Au NT nanohybrid. The o_1-CBT ligand showed sharp peaks, with a missing peak at 133 cm^{-1}, corresponding to the Ag−Ag NC core vibration. As there is no observation of Au−S bond formation, the electrostatic interaction between the slightly positive Au NT (ζ potential of 30 ± 5 mV after two washes in water) and the negatively charged Ag_{17} NC plays the key role in forming the NC−NP nanohybrid while keeping the Ag_{17} intact. The negative ion mode of high-resolution electrospray ionization mass spectrometric studies (Figure S14) showed that Ag_{17} remained unchanged in the nanohybrid in a water/ethanol solvent mixture, with an ion at m/z 1312.42, matching exactly with the parent Ag_{17}, with a −3 charge.[29] No additional peaks from Au−Ag exchange in the Ag_{17}@Au NT nanohybrid, along with the same isotropic distribution pattern, confirmed the structural integrity of the NC. London dispersion forces can also help to stabilize this interaction.[52] Figure S15 shows that nanospheres show less enhancement than NTs, proving that the surface curvature of the NPs plays an important role. A bare Au NT substrate was also measured as a control. It showed no significant Raman peaks, as sufficient centrifugations were performed to remove the excess protecting ligand, cetyltrimethylammonium chloride (CTAC), of the Au NT. The IR spectra of Au NTs before and after washing showed the absence of CTAC features postwashing (Figure S16). This confirms the minimal presence of CTAC, which is sufficient to suppress nanoparticle aggregation while ensuring no detectable Raman contribution from the surfactant. To isolate the contribution of the NC core from that of the ligand, a control experiment was performed by using free o_1-CBT adsorbed on Au NTs under identical conditions. In Figure S17, comparative spectra of free o_1-CBT and the Au NT with o_1-CBT with a

https://doi.org/10.1021/acs.nanolett.5c05462
Nano Lett. XXXX, XXX, XXX−XXX

concentration similar to that of Ag_{17} show that the enhancement is not as high as that of the Ag_{17}@Au NT, confirming the crucial role of the cluster core as an electron reservoir.

Table 1 highlights the peaks corresponding to the Ag_{13} core vibration (Ag−Ag vibrations) and the ligand's different vibrational modes. Although there are many vibrations due to the CB ring, the modes related to Ag−Ag vibrations, cage breathing, and B−H bending are of particular interest due to their sensitivity to changes in the electronic environment.[53−55]

Table 1. Raman Marker Bands and Assignments for the Vibrations of the Free o_1-CBT Ligand

Raman shift (cm^{-1})	spectral assignments	Raman shift (cm^{-1})	spectral assignments
133	Ag_{13} core vibration (Ag−Ag vibrations)	871, 960	BBH bending mode
191, 335, 491	B−B, B−S, and B−C vibrational modes	1038, 1074	skeletal breathing and B−H bending mode
586, 630	BBB breathing mode	1117, 1170	C−H bending mode
678	BBC breathing mode		
724	B−B bending	2618, 2645	B−H stretching mode and contribution of S−H stretching mode
776	icosahedral breathing mode/pulsation of the icosahedral cage	3051, 3070	C−H stretching mode

To determine the Raman enhancement behavior, we measured the SERS intensity as a function of Ag_{17} concentration while keeping the concentrations of Au NTs and laser parameters constant. Figure 3a shows that the marker bands from the CBT shell intensify systematically while positions and line shapes remain almost invariant, indicating nondestructive adsorption of Ag_{17}. Figure 3a shows the concentration-dependent SERS intensity variations of Ag_{17} under the experimental conditions in the presence of the Au NT. Beyond that range, the signal-to-noise ratio became less than 3, and hence, it was not considered for evaluation. Below this threshold, the spectral signal merged with the baseline noise, confirming the statistical limit of SERS detectability under the employed optical configuration. Furthermore, we have calculated the LOD to be 1.64 nM by calibrating the SERS intensities of the 776 cm^{-1} peak for the Ag_{17}@Au NT at 1, 2, 4, 6, 8, and 10 nM. The calibration curve (Figure S18) and the detailed calculations are shown in the Supporting Information, following the standard protocol.[56,57] Experimental data show a gradual increase in intensity as the concentrations of Ag_{17} are changed from as low as 1 nM to 100 μM. Gradual enhancement with an increase in concentration has been demonstrated for the peaks at 129, 776, and 860 cm^{-1} (Ag−Ag stretching, cage breathing, and BBH bending, respectively), as shown in Figure 3b. Variations in Raman amplification across bands reflect mode-specific coupling strengths arising from the complex electronic and geometric structures of the Ag_{17}@Au NT nanohybrid.

To investigate the effect of the cluster core on the vibrational profile of o_1-CBT, we compared the Raman spectra of the free o_1-CBT ligand with those of the Ag_{17} NC. The computed Raman spectra of the Ag_{17} NC reproduced the experimental features with small shifts attributed to gas-phase simulation conditions, validating the computational model (Figure S19). To explore CE, we analyzed the electron density redistribution in the Ag_{17} NC using 12 o_1-CBT ligands in their thiolate form, revealing a reorganization of charge density (Figure 4a). Figure 4b shows the simulated Raman intensities of the o_1-CBT and Ag_{17} NC, confirming the observed Raman spectral intensity amplification. A signal enhancement of $\sim 2 \times 10^2$ from the calculation, with specific vibrations more prominently enhanced, is also consistent with experiments. We also observed a slight shift in the Raman signal of Ag_{17}, indicating a potential electron density redistribution around o_1-CBT. To understand the nonuniformity of the enhancement for various modes, we utilized a model system of $[Ag_{17}(o_1\text{-CBT})]^{3-}$, as shown in Figure S20. The electron density was shifted from the Ag_{17} core to the o_1-CBT ligand, as expected, given that the latter is a highly electronegative ligand.[58] The resulting separation was spatially localized with the most significant changes in electron density observed in the region proximal to the Ag_{17} core. This can increase the local dipole moment and modify the electrostatic environment experienced by atoms involved during vibrations. In contrast, the atoms located farther from the core displayed much smaller variations in electron density, consistent with the short-range nature of electronic coupling between metals and ligands. This potentially explains the greater enhancement of specific

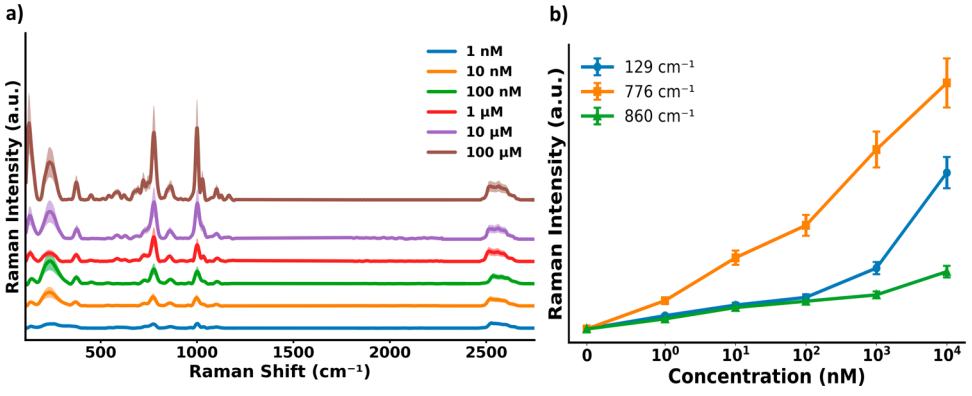

Figure 3. Loading-dependent SERS response of Ag_{17}@Au NTs. (a) Overlaid Raman spectra of the Ag_{17}@Au NT acquired under identical conditions after incubation at increasing Ag_{17} concentrations. (b) Integrated intensities of three representative bands at 129, 776, and 860 cm^{-1} (Ag−Ag vibrations, cage breathing, and BBH bending, respectively) vs Ag_{17} concentration, showing a steady increase. One hundred spectra were collected per sample to calculate the mean and standard deviation.

https://doi.org/10.1021/acs.nanolett.5c05462
Nano Lett. XXXX, XXX, XXX−XXX

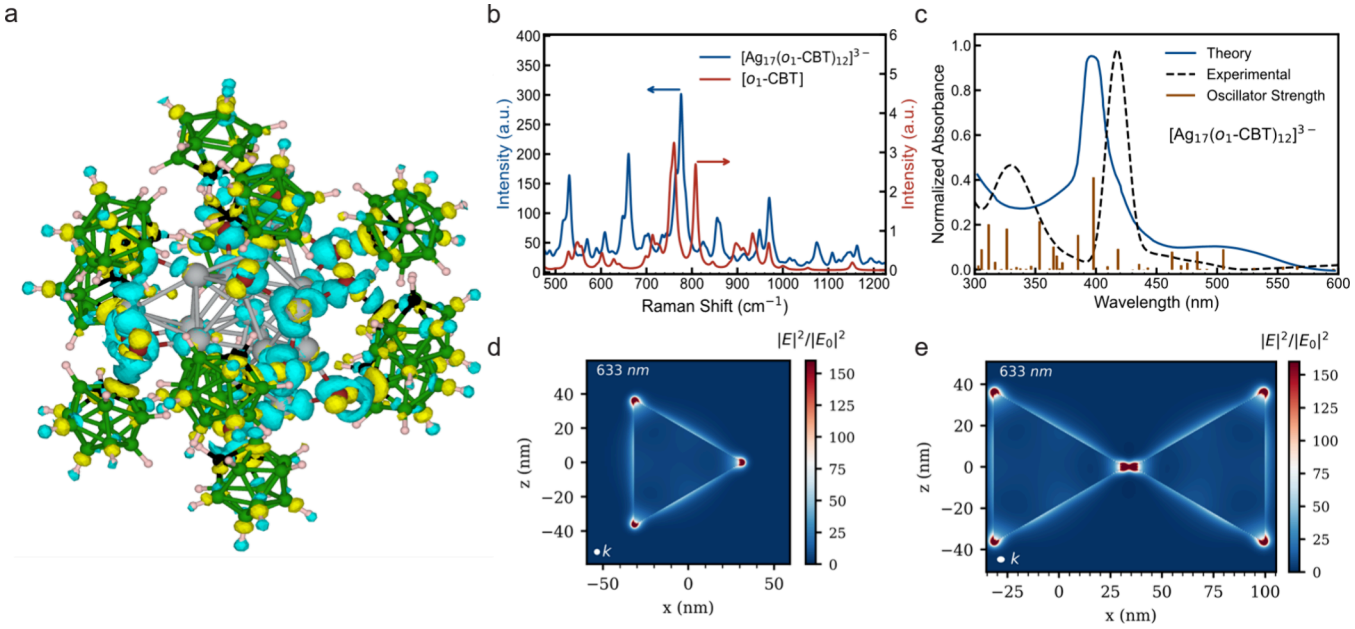

Figure 4. Simulation results. (a) Electron density difference plot of Ag_{17}. Yellow and blue regions correspond to increased and decreased electron density, respectively. Atom colors: green for boron, white for hydrogen, black for carbon, red for sulfur, and metallic gray for silver. (b) Calculated Raman spectra of o_1-CBT and Ag_{17}. (c) Calculated UV−vis absorption spectrum of Ag_{17}. Panels a−c were obtained using TDDFT. Calculated electric field enhancement ($|E|^2/|E_0|^2$) from FDTD simulations for a (d) single Au NT and (e) two Au NTs with an edge length of ∼73 nm separated by 3 nm. Here, $|E|$ and $|E_0|$ represent the amplitudes of the generated and incident electric fields, respectively.

vibrational modes observed experimentally, such as the icosahedral breathing mode and the B−H and C−H bending modes, as shown in Figure 2a. While exploring EM enhancement, TDDFT shows that Ag_{17} lacks resonant transitions at the experimental wavelength of 633 nm as it has an absorption maximum of ∼400 nm. It rules out the possibility of EM from the NC, as shown in Figure 4c. Additionally, the lack of spectral overlap also eliminates the possibility of resonance Raman enhancement, suggesting that the Ag_{17} core aids in the enhancement of the Raman signal, predominantly via the CE mechanism.

Once the role of the Ag_{17} core in o_1-CBT Raman signal enhancement in the NC was understood, the electromagnetic effect imparted by the Au NT was examined. The size of the Au NT was ∼72.5 nm, which lay beyond the scope of DFT and TDDFT. Hence, the role of the plasmonic Au NT was explored using FDTD simulations. The extinction spectrum of the Au NT displayed a plasmonic peak at around 630 nm (Figure S21). ($|E|^2/|E_0|^2$) was used for the local intensity enhancement of the electromagnetic field for mapping the hot spots, whereas the SERS enhancement factor was calculated as ($|E|^4/|E_0|^4$) at a wavelength of 633 nm without considering the Stokes shift. As expected for the Au NT, we observed ∼2×10^2- to 3.43×10^4-fold enhancement in the induced electric field at 633 nm across the surface and at the tips of the triangles (Figure 4d and Figure S22). During the experiment, SERS signals are often dominated by a small number of molecules located at highly localized hot spots, while the majority of surface sites contribute weakly to the measured response.[59] Here, we expect the overall SERS intensity to be an ensemble average over different hot spots, but since we cannot characterize this distribution, the overall enhancement cannot be uniquely quantified. Simulations of a dimer showed the potential for a hot spot in a configuration where the tips of two Au NTs face each other with a 3 nm separation, as shown in Figure 4e. This hot spot is well-suited for trapping Ag_{17} NCs with a diameter of ∼1.7 nm.[29] Experimental observation of Raman signal enhancement is less intense (EF ∼ 10^4) than what we expected using the Au NT dimer. We rationalize the computational results with experimental findings by considering that the organic ligands, CTAC, were excluded from the FDTD simulation to remove complexities. This will increase the distance of Ag_{17} from the Au NT, leading to a smaller enhancement, even with a plasmonic response. Considering the dimer case, although intense, the contribution from such a geometry will be smaller due to the low probability of such a configuration with no explicit experimental control. Based on our results, we propose that control over distance and orientation between different Au NTs will lead to greater enhancement (∼10^5 to ∼10^6). The experimental EF decreases since the ligands are not uniform under a high field intensity. Overall, we found that CE from Ag_{17} and EM enhancement from Au NT lead to the observed enhanced intensity of the Raman signal of o_1-CBT. In short, the EM field concentration of the NT sets the stage, while TDDFT-resolvable CT channels provide the band-specific boosts seen across these canonical experiment−theory pairs.

In summary, we established atomically precise NCs as intrinsic SERS probes when coupled with Au NTs, uncovering charge-transfer-mediated enhancement through o_1-CBT ligands while reaffirming their molecular identity. We develop a mechanistic framework linking quantized charge-transfer states in atomically precise NCs to macroscopic plasmonic enhancement, offering molecular-level insight into SERS amplification pathways. Beyond conventional techniques such as UV−vis, mass spectrometry, and X-ray diffraction, Raman and SERS uniquely capture the vibrational fingerprints of these hybrids, providing direct insight into NC−NP interactions. Comparative experimental and theoretical analyses reveal that Ag_{17} exhibits Raman amplification analogous to molecular

https://doi.org/10.1021/acs.nanolett.5c05462
Nano Lett. XXXX, XXX, XXX−XXX

probes, with ligand dynamics and NC−NP coupling dictating stability and reproducibility. Unlike regular reporter dyes, the o_1-CBT ligand enhances photostability under irradiation, while Ag_{17}@Au NTs synergistically boost CE and EM contributions, yielding intense and stable signals. Such NC−NP nanohybrid platforms establish a design principle for creating a library of NCs as robust SERS reporters, thereby expanding the scope of cluster-based quantum sensing. Importantly, the reproducibility of such NC−NP nanohybrids depends on the stabilization of the interfacial junction, as uncontrolled cluster migration or configurational drift can change the intrinsic charge-transfer signatures. Rational interface engineering, including molecular tethering, directed surface functionalization, protective encapsulation, and ligand-shell modulation, can produce better nanohybrids. They represent practical routes to minimize spectral dispersion while preserving the electromagnetic−chemical synergy, thereby increasing the likelihood of using NCs as stable SERS probes.

■ ASSOCIATED CONTENT

Data Availability Statement

The data that support the findings of the study are included in the published article and its Supporting Information.

Supporting Information

The Supporting Information is available free of charge at https://pubs.acs.org/doi/10.1021/acs.nanolett.5c05462.

Experimental details, synthesis and characterization of Au NTs and the Ag_{17} NC, fabrication of the Ag_{17}@Au NT nanohybrid, Raman calibration and enhancement factor analysis, reproducibility and photostability studies, PCA and PLS-based quantitative analysis and detection limit estimation, DFT and TDDFT calculations of the Raman spectra of NC, and FDTD simulations of the plasmonic response and field enhancement in Au NTs (PDF)

■ AUTHOR INFORMATION

Corresponding Authors

Thalappil Pradeep − *DST Unit of Nanoscience (DST UNS) and Thematic Unit of Excellence (TUE), Department of Chemistry, Indian Institute of Technology Madras, Chennai 600036, India; International Centre for Clean Water, IIT Madras Research Park, Chennai 600113, India;* orcid.org/0000-0003-3174-534X; Email: pradeep@iitm.ac.in

George C. Schatz − *Department of Chemical & Biological Engineering, Northwestern University, Evanston, Illinois 60208, United States; Department of Chemistry and International Institute for Nanotechnology, Northwestern University, Evanston, Illinois 60208, United States;* orcid.org/0000-0001-5837-4740; Email: g-schatz@northwestern.edu

Tomas Base − *Department of Syntheses, Institute of Inorganic Chemistry, The Czech Academy of Sciences, Rez 25068, Czech Republic;* orcid.org/0000-0003-2533-8705; Email: tbase@iic.cas.cz

Authors

Sujan Manna − *DST Unit of Nanoscience (DST UNS) and Thematic Unit of Excellence (TUE), Department of Chemistry, Indian Institute of Technology Madras, Chennai 600036, India*

Anant O. Bhasin − *Department of Chemistry, Brandeis University, Waltham, Massachusetts 02453, United States;* orcid.org/0009-0000-8042-7466

Vivek Yadav − *DST Unit of Nanoscience (DST UNS) and Thematic Unit of Excellence (TUE), Department of Chemistry, Indian Institute of Technology Madras, Chennai 600036, India;* orcid.org/0009-0004-0244-0541

Soham Chowdhury − *DST Unit of Nanoscience (DST UNS) and Thematic Unit of Excellence (TUE), Department of Chemistry, Indian Institute of Technology Madras, Chennai 600036, India;* orcid.org/0009-0000-8151-6065

Subrata Duary − *DST Unit of Nanoscience (DST UNS) and Thematic Unit of Excellence (TUE), Department of Chemistry, Indian Institute of Technology Madras, Chennai 600036, India*

Samapti Mondal − *DST Unit of Nanoscience (DST UNS) and Thematic Unit of Excellence (TUE), Department of Chemistry, Indian Institute of Technology Madras, Chennai 600036, India*

Sajal Kumar Giri − *Department of Chemical Sciences, Indian Institute of Science Education and Research (IISER) Mohali, Mohali, Punjab 140306, India;* orcid.org/0000-0001-9145-6801

Complete contact information is available at: https://pubs.acs.org/10.1021/acs.nanolett.5c05462

Author Contributions

A.O.B. and V.Y. contributed equally to this work. Sujan Manna was responsible for the conception and design of the work, performed the experiments, analyzed the data, and prepared the manuscript. A.O.B. performed the computational analysis, and S.K.G. guided him. V.Y. helped with the synthesis of the nanocluster. S.C. performed the XPS. S.D. performed the IR and photoluminescence experiments. Samapti Mondal performed mass spectrometry. T.B. synthesized the carborane-thiols used in this work and conducted all of the work relating to those systems. G.C.S. guided the TDDFT part. T.P. supervised the study and improved the manuscript.

Notes

The authors declare no competing financial interest.

■ ACKNOWLEDGMENTS

The authors thank the Department of Science and Technology, Government of India, and IIT Madras for supporting our research. T.P. thanks the Science and Engineering Research Board (SERB), India, for funding through the SPR/2021/000439 research grant, the SUPRA project, and the J. C. Bose Fellowship. T.P. acknowledges funding from the Centre of Excellence (CoE) on Molecular Materials and Functions from the Institute of Eminence scheme of IIT Madras. A.O.B. acknowledges National Science Foundation (NSF) Grant CHE-2046099, and G.C.S. acknowledges NSF Grant CHE-2347622. Computational work was performed on the Brandeis HPCC, which is partially supported by the NSF through DMR-MRSEC 2011846 and OAC-1920147. S.M. thanks the UGC for his research fellowship.

■ REFERENCES

(1) Langer, J.; Jimenez de Aberasturi, D.; Aizpurua, J.; Alvarez-Puebla, R. A.; Auguié, B.; Baumberg, J. J.; Bazan, G. C.; Bell, S. E. J.;

Boisen, A.; Brolo, A. G.; et al. Present and Future of Surface-Enhanced Raman Scattering. *ACS Nano* **2020**, *14* (1), 28−117.
(2) Yi, J.; You, E.-M.; Hu, R.; Wu, D.-Y.; Liu, G.-K.; Yang, Z.-L.; Zhang, H.; Gu, Y.; Wang, Y.-H.; Wang, X.; et al. Surface-Enhanced Raman Spectroscopy: A Half-Century Historical Perspective. *Chem. Soc. Rev.* **2025**, *54* (3), 1453−1551.
(3) Stiles, P. L.; Dieringer, J. A.; Shah, N. C.; Van Duyne, R. P. Surface-Enhanced Raman Spectroscopy. *Annu. Rev. Anal. Chem.* **2008**, *1* (1), 601−626.
(4) Liang, X.; Liang, B.; Pan, Z.; Lang, X.; Zhang, Y.; Wang, G.; Yin, P.; Guo, L. Tuning Plasmonic and Chemical Enhancement for SERS Detection on Graphene-Based Au Hybrids. *Nanoscale* **2015**, *7* (47), 20188−20196.
(5) Valley, N.; Greeneltch, N.; Van Duyne, R. P.; Schatz, G. C. A Look at the Origin and Magnitude of the Chemical Contribution to the Enhancement Mechanism of Surface-Enhanced Raman Spectroscopy (SERS): Theory and Experiment. *J. Phys. Chem. Lett.* **2013**, *4* (16), 2599−2604.
(6) Lombardi, J. R.; Birke, R. L. A Unified View of Surface-Enhanced Raman Scattering. *Acc. Chem. Res.* **2009**, *42* (6), 734−742.
(7) Morton, S. M.; Jensen, L. Understanding the Molecule-Surface Chemical Coupling in SERS. *J. Am. Chem. Soc.* **2009**, *131* (11), 4090−4098.
(8) Ji, W.; Li, L.; Song, W.; Wang, X.; Zhao, B.; Ozaki, Y. Enhanced Raman Scattering by ZnO Superstructures: Synergistic Effect of Charge Transfer and Mie Resonances. *Angew. Chem., Int. Ed.* **2019**, *58* (41), 14452−14456.
(9) Wang, X.; Shi, W.; Wang, S.; Zhao, H.; Lin, J.; Yang, Z.; Chen, M.; Guo, L. Two-Dimensional Amorphous TiO2 Nanosheets Enabling High-Efficiency Photoinduced Charge Transfer for Excellent SERS Activity. *J. Am. Chem. Soc.* **2019**, *141* (14), 5856−5862.
(10) Zhang, Y.; Shi, Z.; Cui, H.; Xia, Q.; Liu, F.; Wang, Z.; Wang, J.; Fan, H.; Shu, C.; Chen, B.; Li, H.; Lai, Z.; Luo, Z.; Zheng, W.; Wang, L.; Huang, Z. Phase-Engineered Transition Metal Dichalcogenides for Highly Efficient Surface-Enhanced Raman Scattering. *Nano Lett.* **2024**, *24* (45), 14293−14301.
(11) Tavakkoli Yaraki, M.; Rubio, N. S.; Tukova, A.; Liu, J.; Gu, Y.; Kou, L.; Wang, Y. Spectroscopic Identification of Charge Transfer of Thiolated Molecules on Gold Nanoparticles via Gold Nanoclusters. *J. Am. Chem. Soc.* **2024**, *146* (9), 5916−5926.
(12) Jin, R.; Zeng, C.; Zhou, M.; Chen, Y. Atomically Precise Colloidal Metal Nanoclusters and Nanoparticles: Fundamentals and Opportunities. *Chem. Rev.* **2016**, *116* (18), 10346−10413.
(13) Pradeep, T. *Atomically Precise Metal Nanoclusters*; Elsevier, 2022.
(14) Chakraborty, I.; Pradeep, T. Atomically Precise Clusters of Noble Metals: Emerging Link between Atoms and Nanoparticles. *Chem. Rev.* **2017**, *117* (12), 8208−8271.
(15) Jena, P.; Sun, Q. Super Atomic Clusters: Design Rules and Potential for Building Blocks of Materials. *Chem. Rev.* **2018**, *118* (11), 5755−5870.
(16) Jin, R. Atomically Precise Metal Nanoclusters: Stable Sizes and Optical Properties. *Nanoscale* **2015**, *7* (5), 1549−1565.
(17) Kang, X.; Zhu, M. Tailoring the Photoluminescence of Atomically Precise Nanoclusters. *Chem. Soc. Rev.* **2019**, *48* (8), 2422−2457.
(18) Chen, T.; Lin, H.; Cao, Y.; Yao, Q.; Xie, J. Interactions of Metal Nanoclusters with Light: Fundamentals and Applications. *Adv. Mater.* **2022**, *34* (25), 2103918.
(19) Zhong, Y.; Wu, Z.; Bai, X.; Zhang, Y.; Xie, J. Viewing Inorganic Metal Nanoclusters through the Lens of Molecular Chemistry. *Mater. Today* **2024**, *76*, 72−93.
(20) Cerretani, C.; Kanazawa, H.; Vosch, T.; Kondo, J. Crystal Structure of a NIR-Emitting DNA-Stabilized Ag16 Nanocluster. *Angew. Chem., Int. Ed.* **2019**, *58* (48), 17153−17157.
(21) Han, Z.; Dong, X.-Y.; Luo, P.; Li, S.; Wang, Z.-Y.; Zang, S.-Q.; Mak, T. C. W. Ultrastable Atomically Precise Chiral Silver Clusters with More than 95% Quantum Efficiency. *Sci. Adv.* **2020**, *6* (6), No. eaay0107.
(22) Yang, H.; Lei, J.; Wu, B.; Wang, Y.; Zhou, M.; Xia, A.; Zheng, L.; Zheng, N. Crystal Structure of a Luminescent Thiolated Ag Nanocluster with an Octahedral Ag64+ Core. *Chem. Commun.* **2013**, *49* (3), 300−302.
(23) Jana, A.; Unnikrishnan, P. M.; Poonia, A. K.; Roy, J.; Jash, M.; Paramasivam, G.; Machacek, J.; Adarsh, K. N. V. D.; Base, T.; Pradeep, T. Carboranethiol-Protected Propeller-Shaped Photoresponsive Silver Nanomolecule. *Inorg. Chem.* **2022**, *61* (23), 8593−8603.
(24) Joshi, C. P.; Bootharaju, M. S.; Alhilaly, M. J.; Bakr, O. M. [Ag25(SR)18]-: The "Golden" Silver Nanoparticle. *J. Am. Chem. Soc.* **2015**, *137* (36), 11578−11581.
(25) AbdulHalim, L. G.; Bootharaju, M. S.; Tang, Q.; Del Gobbo, S.; AbdulHalim, R. G.; Eddaoudi, M.; Jiang, D.; Bakr, O. M. Ag29(BDT)12(TPP)4: A Tetravalent Nanocluster. *J. Am. Chem. Soc.* **2015**, *137* (37), 11970−11975.
(26) Guan, Z.-J.; Zeng, J.-L.; Nan, Z.-A.; Wan, X.-K.; Lin, Y.-M.; Wang, Q.-M. Thiacalix[4]Arene: New Protection for Metal Nanoclusters. *Sci. Adv.* **2016**, *2* (8), No. e1600323.
(27) Yang, H.; Wang, Y.; Chen, X.; Zhao, X.; Gu, L.; Huang, H.; Yan, J.; Xu, C.; Li, G.; Wu, J.; Edwards, A. J.; Dittrich, B.; Tang, Z.; Wang, D.; Lehtovaara, L.; Häkkinen, H.; Zheng, N. Plasmonic Twinned Silver Nanoparticles with Molecular Precision. *Nat. Commun.* **2016**, *7* (1), 12809.
(28) Alam, N.; Kumar Das, A.; Chandrashekar, P.; Baidya, P.; Mandal, S. Recent Progress in Atomically Precise Silver Nanocluster-Assembled Materials. *Nanoscale* **2024**, *16*, 10087.
(29) Yadav, V.; Jana, A.; Acharya, S.; Malola, S.; Nagar, H.; Sharma, A.; Kini, A. R.; Antharjanam, S.; Machacek, J.; Adarsh, K. N. V. D.; Base, T.; Häkkinen, H.; Pradeep, T. Site-Specific Substitution in Atomically Precise Carboranethiol-Protected Nanoclusters and Concomitant Changes in Electronic Properties. *Nat. Commun.* **2025**, *16* (1), 1197.
(30) Jana, A.; Jash, M.; Ahmed Dar, W.; Roy, J.; Chakraborty, P.; Paramasivam, G.; Lebedkin, S.; Kirakci, K.; Manna, S.; Antharjanam, S.; Machacek, J.; Kucerakova, M.; Ghosh, S.; Lang, K.; Kappes, M. M.; Base, T.; Pradeep, T. Carborane-Thiol Protected Copper Nanoclusters: Stimuli-Responsive Materials with Tunable Phosphorescence. *Chem. Sci.* **2023**, *14* (6), 1613−1626.
(31) Jankowiak, A.; Kaszyński, P. Practical Synthesis of 1,12-Difunctionalized *o* -Carborane for the Investigation of Polar Liquid Crystals. *Inorg. Chem.* **2014**, *53* (16), 8762−8769.
(32) Grimes, R. N. Boron Clusters Come of Age. *J. Chem. Educ.* **2004**, *81* (5), 657.
(33) Leites, L. A. Vibrational Spectroscopy of Carboranes and Parent Boranes and Its Capabilities in Carborane Chemistry. *Chem. Rev.* **1992**, *92* (2), 279−323.
(34) Park, K.; Pederson, M. R.; Boyer, L. L.; Mei, W. N.; Sabirianov, R. F.; Zeng, X. C.; Bulusu, S.; Curran, S.; Dewald, J.; Day, E.; Adenwalla, S.; Diaz, M.; Rosa, L. G.; Balaz, S.; Dowben, P. A. Electronic Structure and Vibrational Spectra of ${\mathrm{C}}_{2}{\mathrm{B}}_{10}$-Based Clusters and Films. *Phys. Rev. B* **2006**, *73* (3), 035109.
(35) Scarabelli, L.; Coronado-Puchau, M.; Giner-Casares, J. J.; Langer, J.; Liz-Marzán, L. M. Monodisperse Gold Nanotriangles: Size Control, Large-Scale Self-Assembly, and Performance in Surface-Enhanced Raman Scattering. *ACS Nano* **2014**, *8* (6), 5833−5842.
(36) Kuwahara, S.; Narita, Y.; Mizuno, L.; Kurotsu, H.; Yoshino, H.; Kuwahara, M. Localized Surface Plasmon Resonance-Induced Welding of Gold Nanotriangles and the Local Plasmonic Properties for Multicolor Sensing and Light-Harvesting Applications. *ACS Appl. Nano Mater.* **2020**, *3* (6), 5172−5177.
(37) Son, J.; Kim, G.-H.; Lee, Y.; Lee, C.; Cha, S.; Nam, J.-M. Toward Quantitative Surface-Enhanced Raman Scattering with Plasmonic Nanoparticles: Multiscale View on Heterogeneities in Particle Morphology, Surface Modification, Interface, and Analytical Protocols. *J. Am. Chem. Soc.* **2022**, *144* (49), 22337−22351.

https://doi.org/10.1021/acs.nanolett.5c05462
Nano Lett. XXXX, XXX, XXX−XXX

(38) Tian, F.; Bonnier, F.; Casey, A.; Shanahan, A. E.; Byrne, H. J. Surface Enhanced Raman Scattering with Gold Nanoparticles: Effect of Particle Shape. *Anal. Methods* **2014**, *6* (22), 9116−9123.
(39) Tiwari, V. S.; Oleg, T.; Darbha, G. K.; Hardy, W.; Singh, J. P.; Ray, P. C. Non-Resonance SERS Effects of Silver Colloids with Different Shapes. *Chem. Phys. Lett.* **2007**, *446* (1), 77−82.
(40) Huang, Y.-F.; Wu, D.-Y.; Zhu, H.-P.; Zhao, L.-B.; Liu, G.-K.; Ren, B.; Tian, Z.-Q. Surface-Enhanced Raman Spectroscopic Study of p-Aminothiophenol. *Phys. Chem. Chem. Phys.* **2012**, *14* (24), 8485−8497.
(41) Sprague-Klein, E. A.; Negru, B.; Madison, L. R.; Coste, S. C.; Rugg, B. K.; Felts, A. M.; McAnally, M. O.; Banik, M.; Apkarian, V. A.; Wasielewski, M. R.; Ratner, M. A.; Seideman, T.; Schatz, G. C.; Van Duyne, R. P. Photoinduced Plasmon-Driven Chemistry in Trans-1,2-Bis(4-Pyridyl)Ethylene Gold Nanosphere Oligomers. *J. Am. Chem. Soc.* **2018**, *140* (33), 10583−10592.
(42) Neupane, G. P.; Salaria, R. K. Improving SERS Sensitivity via Hot Spots and Control of Molecular Orientation. *J. Mater. Chem. C* **2026**, *14* (3), 1244−1252.
(43) Scher, K. M. R.; Wang, Z.; Nair, A.; Wu, Y.; Bartoli, M.; Rovere, M.; Tagliaferro, A.; Rangan, S.; Wang, L.; Fabris, L. Concentration and Surface Chemistry Dependent Analyte Orientation on Nanoparticle Surfaces. *J. Phys. Chem. C* **2022**, *126* (38), 16499−16513.
(44) Song, J.; Nam, W.; Zhou, W. Scalable High-Performance Nanolaminated SERS Substrates Based on Multistack Vertically Oriented Plasmonic Nanogaps. *Adv. Mater. Technol.* **2019**, *4* (5), 1800689.
(45) Deriu, C.; Fabris, L. A Surface Chemistry Perspective on SERS: Revisiting the Basics to Push the Field Forward. *Chem. Soc. Rev.* **2025**, *54* (11), 5224−5247.
(46) Chakraborty, A.; Manna, S.; Mondal, B.; Bodiuzzaman, M.; Nagar, A.; Chowdhury, S.; Nayak, T.; Nonappa; Pradeep, T. Morphology-Preserved Alloying in Anisotropic Gold Nanoparticles Using Atomically Precise Nanoclusters. *Small* **2025**, *21* (43), 2410784.
(47) Trinh, H. D.; Yoon, S. Silica-Encapsulated Core-Satellite Gold Nanoparticle Assemblies as Stable, Sensitive, and Multiplex Surface-Enhanced Raman Scattering Probes. *ACS Appl. Nano Mater.* **2022**, *5* (4), 5087−5095.
(48) Zhang, Y.; Li, X.; Xue, B.; Kong, X.; Liu, X.; Tu, L.; Chang, Y. A Facile and General Route to Synthesize Silica-Coated SERS Tags with the Enhanced Signal Intensity. *Sci. Rep.* **2015**, *5* (1), 14934.
(49) Scarabelli, L.; Liz-Marzán, L. M. An Extended Protocol for the Synthesis of Monodisperse Gold Nanotriangles. *ACS Nano* **2021**, *15* (12), 18600−18607.
(50) Castner, D. G.; Hinds, K.; Grainger, D. W. X-Ray Photoelectron Spectroscopy Sulfur 2p Study of Organic Thiol and Disulfide Binding Interactions with Gold Surfaces. *Langmuir* **1996**, *12* (21), 5083−5086.
(51) Lorén, A.; Engelbrektsson, J.; Eliasson, C.; Josefson, M.; Abrahamsson, J.; Johansson, M.; Abrahamsson, K. Internal Standard in Surface-Enhanced Raman Spectroscopy. *Anal. Chem.* **2004**, *76* (24), 7391−7395.
(52) Li, G.; Tamblyn, I.; Cooper, V. R.; Gao, H.-J.; Neaton, J. B. Molecular Adsorption on Metal Surfaces with van Der Waals Density Functionals. *Phys. Rev. B* **2012**, *85* (12), 121409.
(53) Salam, A.; Deleuze, M. S.; François, J.-P. Computational Study of the Structural and Vibrational Properties of Ten and Twelve Vertex *Closo*-Carboranes. *Chem. Phys.* **2003**, *286* (1), 45−61.
(54) Jana, A.; Yadav, V.; Kučeráková, M.; Malola, S.; Kini, A. R.; Acharya, S.; Poonia, A. K.; Macháček, J.; Adarsh, K. N. V. D.; Häkkinen, H.; Base, T.; Pradeep, T. $[Ag_{62}\ S_{12}\ (CBT)_{32}]^{4+}$: A 2.2 Nm Two-Electron Superatomic Carborane-Thiolated Silver Nanocluster Exhibiting Multilayer Charge Separation. *ACS Nano* **2025**, *19* (39), 35015−35026.
(55) Leites, L. A.; Vinogradova, L. E.; Aleksanyan, V. T.; Bukalov, S. S. Vibrational Spectra of O-, m-, and p-Carboranes B10H10C2H2 and Their B-Decachloro-Substitution Products. *Bull. Acad. Sci. USSR Div. Chem. Sci.* **1976**, *25* (11), 2311−2317.
(56) Long, G. L.; Winefordner, J. D. Limit of Detection. A Closer Look at the IUPAC Definition. *Anal. Chem.* **1983**, *55* (7), 712A−724A.
(57) Hubaux, A.; Vos, G. Decision and Detection Limits for Calibration Curves. *Anal. Chem.* **1970**, *42* (8), 849−855.
(58) Godovikov, N. N.; Balema, V. P.; Rys, E. G. Carborane-Containing Organophosphorus Compounds. Synthesis and Properties. *Russ. Chem. Rev.* **1997**, *66* (12), 1017−1032.
(59) Fang, Y.; Seong, N.-H.; Dlott, D. D. Measurement of the Distribution of Site Enhancements in Surface-Enhanced Raman Scattering. *Science* **2008**, *321* (5887), 388−392.

https://doi.org/10.1021/acs.nanolett.5c05462
Nano Lett. XXXX, XXX, XXX−XXX